VII International Conference on Computational Methods in Marine Engineering
MARINE 2017
M. Visonneau, P. Queutey and D. Le Touzé (Eds)

HYBRIDIZATION OF FINITE ELEMENT-BOUNDARY ELEMENT METHODS USING AN ABSORBING BOUNDARY CONDITION FOR VIBRO-ACOUSTIC UNDERWATER NOISE SIMULATIONS

MARINE 2017

N. ZERBIB†, K. BOUAYED†, J. LEFEVBRE†, M. ANCIANT†, L. MEBAREK†

† ESI Group, Center of Excellence Vibro-Acoustics
8, rue Clement Bayard
60200, Compiegne, France
email: nicolas.zerbib@esi-group.com, www.esi-group.com

Key words: Fluid Structure Interaction, Underwater, Added Mass, Sub-structuring, Finite Element Method, Boundary Element Method, MultiLevel Fast Multipole Method, Hybridization, Adaptive Absorbing Boundary Condition

Abstract. Sound propagation from industrial activities in underwater or estimation of the target strength of waterside security systems are considered immensely important by many scientists for both regulators of development projects or military aspects. This paper presents a comparison of numerical methods used to model large scale acoustic coupled fluid structure interaction underwater problems. Concerning the mechanical behavior of the structure, it is absolutely essential during the computation of the modal basis to take into account the added mass effect of the heavy fluid, the water, around the structure. In that work, the added mass matrix is evaluated by a Boundary Element Method and the modal basis is computed by a sub-structuring algorithm to deal with both large number of degrees of freedom and modes. On the acoustic point of view, this article presents an efficient way to deal with very complex and large scale underwater target. This method is competing against standard Perfectly Match Layers (PML), Infinite Element Method (IEM), standard Boundary Element Method (BEM) and more recently the coupled MultiLevel Fast Multipole Method (MLFMM). Reducing considerably both computational time and RAM requirement keeping a very good accuracy, this approach hybridizes advantages of FEM, BEM and MLFMM methods through a domain decomposition technic using an Adaptive Absorbing Boundary Condition (AABC). Some numerical results are presented to present the capabilities of that approach on academic cases but also on more industrial applications.

1 INTRODUCTION

Predicting the vibro-acoustic responses of thin shell structures in contact with an unbounded fluid is important in various engineering applications including underwater vehicles and submarines. Low frequency vibration modes of a thin shell can be easily excited by external forces for example, which may result in a high level of radiated noise. Identifying the modal contributions to the sound radiation of shell structures is useful to reduce the noise by refining the design of the structure. For an elastic shell in air, the structural and acoustic responses can be subsequently solved. However, for the case of a shell immersed in water where the fluid

impedance is comparable to that of the shell, the fluid-structure interaction is strongly coupled and the structural and acoustic responses have to be simultaneously solved.

1.1 The Target Strength

An acoustic scattering signature is the Target Strength (TS) of an object, Eq (1), that has been impinged on a broad band of frequencies and, for each frequency, over a broad range of aspect angles. When the obstacle is impinged on a plane wave (wave fronts are planar, rather than curved, as occurs when the sound source is far away from the object), the TS is defined as

$$\boldsymbol{S(\alpha,\beta) = \lim_{r\to\infty} 10 \log_{10}\left(\frac{\|r - r_0\|^2 p_s{}^2(r,\alpha,\beta)}{p_i{}^2(r_0,\alpha_i,\beta_i)}\right)} \quad (1)$$

with $\boldsymbol{p_s(r,\alpha,\beta)}$ denoting the scattered acoustic pressure at range $\boldsymbol{r}$ and $\boldsymbol{p_i(r_0,\alpha_i,\beta_i)}$ the incident field at the geometric location of the center of the target, which is conveniently set to the origin i.e. $\boldsymbol{r_0 = 0}$. This is evaluated in the farfield i.e. $\boldsymbol{r \gg L^2/\lambda}$, with $\boldsymbol{L}$ denoting the characterisitic length of the target and $\boldsymbol{\lambda}$ the acoustic wavelength. In the farfield $\boldsymbol{TS}$ is not dependent on range $\boldsymbol{r}$, $\boldsymbol{\alpha}$ is the aspect angle and $\boldsymbol{\beta}$ the elevation angle as depicted in Fig. 1. For monostatic TS, the incident and "scattered" angles, respectively in light green and in orange as depicted Fig. 1, are equal i.e. $\boldsymbol{(\alpha_i = \alpha, \beta_i = \beta)}$. The aspect angle $\boldsymbol{\alpha}$ is usually the azimuthal angle, which is a horizontal angle about the vertical to the ocean bottom. The elevation angle $\boldsymbol{\beta}$ is the angle between the horizontal plane and the line of sight, measured in the vertical plane. The elevation angle $\boldsymbol{\beta}$ is positive above the horizon ($\boldsymbol{0°}$ elevation angle) and negative below the horizon.

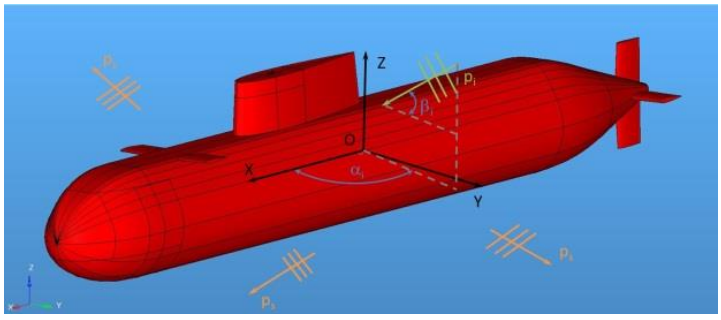

Figure 1: The General Problem of Scattering Strength.

In order to have access to the acoustic scattering signature of their system, one could perform experiments on actual objects. But experiments are expensive and time consuming so only a few can be performed and one cannot perform experiments on unavailable objects or environments. Computers, however, can model virtually any object/environment scenario of interest, including non-existent scenarios. The cost of computer resources per model is negligible compared to that of a real underwater experiment and often faster by orders or magnitude, sometimes enabling hundreds or thousands of templates to be computed in the same time as performing one underwater experiment. There is clearly a need for a computer simulation system that is both high-fidelity and computationally fast. The principle challenges for developing such a system are as follows:

- Multiscale spatially: From small details in the objects (cm) to large distances in the ocean (km).
- Broadband: A five-octave range, $\boldsymbol{kL = 1}$ to $\boldsymbol{kL = 1000}$ where $\boldsymbol{kL}$ is dimensionless frequency, $\boldsymbol{k}$ is the wavenumber ($\boldsymbol{k = 2\pi/\lambda}$), $\boldsymbol{\lambda}$ is the wavenumber of the impinging plane wave and $\boldsymbol{L}$ is the characteristic length of the target.
- A need for extraordinarily high computational efficiency: One acoustic signature template requires sweeping typically over several hundred frequencies, and, for each frequency, several hundred aspect angles, requiring $\boldsymbol{O(10^5)}$ 3-D models.

In the field of computational structural acoustics, the problem of efficiently and as quickly as possible modelling the acoustic field in large exterior domains has remained a difficult challenge for over a quarter century. The coupled Finite Element Method/Boundary Element Method is a very powerful and the most popular tool for computing the vibro-acoustic responses of fluid-loaded structures [4-8]. The FEM method is generally employed to describe the dynamic behavior of the structure whereas the BEM method is used to represent the fluid domain and predict the acoustic responses. This approach produces a deterministic prediction of acceleration, force and stress in the structure. It reveals itself very accurate at low frequency and is still very meaningful across all the spectrum of interest of the vibro-acoustic response. Because BEM matrices tend to be fully populated rather than banded as in FEM, the computational effort to assemble the equations and solve the linear system can be significant. In BEM computations, the CPU time scales with the number of degrees-of-freedom $\boldsymbol{N}$ as $\boldsymbol{O(N^3)}$ and the memory required as $\boldsymbol{O(N^2)}$. Numerical models with typical sizes, analyzed within the frequencies of interest, require long computation times. This precludes the recurrent application of the FEM/BEM approach as new versions of the model design emerge since the early phases, as well as carrying out multiple iterations for optimizing it. Moreover, a modelling overhead is imposed in which the BEM mesh is created based on system-level FEM meshes but made coarser in order to yielding acceptable computation times.

More recently, the coupled Multilevel Fast Multipole Method (MLFMM) [reference ESA/ESTEC] enables to considerably accelerate FEM-BEM computations, without loss of accuracy. It consists of an iterative multi-scale hierarchical clustering of the acoustic sources forming the BEM mesh and allows for a drastic simplification of the long distance interactions. The MLFMM reduces scaling laws with respect to memory and run-time from $\boldsymbol{O(N^3)}$ and $\boldsymbol{O(N^2)}$ in the standard BEM down to $\boldsymbol{O(N_{iter} * N * log^2(N))}$ and $\boldsymbol{N * log^2(N)}$. $\boldsymbol{N_{iter}}$ is the number of iterations in the solver which can be kept sufficiently low for most of the applications of interest. Nevertheless, this approach has also several weaknesses. The main constraint of this method is it relies on an iterative solver. The convergence can be very slow (or not converged at all) because of the complexity of the physics even by using some advanced preconditionner technics like ILUT or SPAI, the quality and the number of nodes of the mesh and the frequency. Even if some preconditioner techniques have been developed, the number of iterations $\boldsymbol{N_{iter}^{FMM}}$ can be very large or infinite for some cases. Moreover, as with every iterative solver, it is not really adapted to deal with a very large number of load cases even if some techniques have been developed to treat this kind of application. In conclusion, this method is not really adapted to compute monostatic TS needing a very large number of plane waves for very complex structure

like a submarine for example. Consequently, a numerical method that is applicable at all frequency and dimension ranges of target is proposed in this paper for fully coupled vibro-acoustic problems keeping advantages of all the standard methods by hybridization of those method by a Domain Decomposition Method (DDM) with overlapping.

2 THE GENERAL COUPLED VIBRO-ACOUSTIC FLUID-STRUCTURE PROBLEM

We consider an elastic structure $\boldsymbol{\Omega_s}$ located in a domain $\boldsymbol{\Omega_f}$ filled by a perfect fluid. We define by $\boldsymbol{\Sigma_s = \partial\Omega_s}$ and $\boldsymbol{\Sigma_f = \partial\Omega_f}$ their respective surfaces. We denote by $\boldsymbol{n}$ the surface unit normal vector oriented inward the fluid domain $\boldsymbol{\Omega_f}$. This elastic structure can be a submarine for example as illustrated on Fig. 2 or a ship hull. This structure can be submitted to an acoustic incident pressure field $\boldsymbol{p^{inc}}$ or a mechanical force $\boldsymbol{f}$.

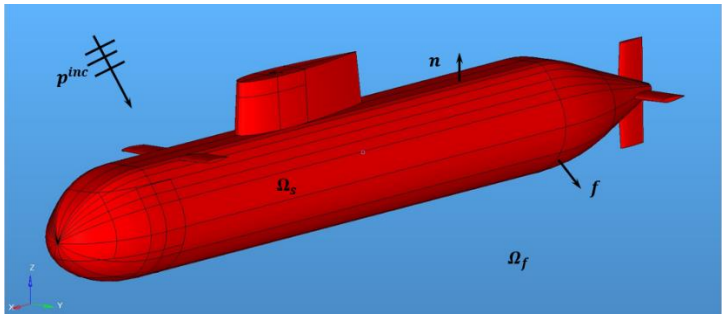

Figure 2: Elastic structure $\boldsymbol{\Omega_s}$ located in a domain $\boldsymbol{\Omega_f}$ filled by a perfect fluid.

The coupled vibro-acoustic fluid-structure problem consists then in solving simultaneously two physical problems:

1. In the first one, a pressure field $\boldsymbol{p}$ is imposed by the fluid on the surface $\boldsymbol{\Sigma_s}$ of the elastic structure
2. In the second one, a displacement field $\boldsymbol{w}$ is imposed on the surface $\boldsymbol{\Sigma_f}$ in the fluid domain from the structure.

The structure behavior obeys to the well-known linear elasticity laws in the harmonic domain at the $\boldsymbol{\omega}$ pulsation for the conservation of the quantity of movement:

$$\boldsymbol{\sigma_{ij,j} - \rho_s\omega^2 w = 0 \qquad in\ \Omega_s} \tag{2}$$

where $\boldsymbol{\rho_s}$ is the volumic mass of the structure, $\boldsymbol{w}$ the displacement and $\boldsymbol{\sigma_{ij}}$ the tensor of stress. We define by the compatibility relation the tensor of constrain as follow:

$$\boldsymbol{\varepsilon_{kl} = \frac{1}{2}(w_{k,l} + w_{l,k})} \tag{3}$$

We also define the behavior law in isotropic linear elasticity by

$$\boldsymbol{\sigma_{ij} = C_{ijkl}\varepsilon_{kl}} \tag{4}$$

where the elasticity modules verify the identities $C_{ijkl} = C_{klij} = C_{jikl} = C_{ijlk}$ (C is the elasticity tensor). Finally, the boundary condition on the surface Σ_s of the elastic structure is defined by

$$\sigma_{ij} n_j = f_i \tag{5}$$

Concerning the fluid, we consider the propagation of time harmonic acoustic waves in a homogeneous isotropic acoustic medium (which can be either finite or infinite) as described by the well-known Helmholtz equation:

$$\nabla^2 p(x) + k^2 p(x) = 0 \qquad in\ \Omega_f \tag{6}$$

where p is the pressure field in the fluid domain, $k = \omega/c$ is the wave number, ω is the angular frequency and c is the wave speed in the acoustic medium whose density is denoted by ρ_f. For the coupling part between these two physics at the fluid-structure interface, the fluid being non-viscous, it does not adhere to the surface, which leads to:

- Continuity to the normal constrains:

$$\sigma_{ij}.n = -p\delta_{ij}.n_i \qquad on\ \Sigma_s \tag{7}$$

- Continuity of the normal displacements:

$$\frac{\partial p}{\partial n} = \rho_f \omega^2 w \quad on\ \Sigma_f \tag{8}$$

Finally, the formulation for the coupled vibro-acoustic fluid-structure problem, expressed in terms of displacements for the structure and pressure for the fluid is

$$\begin{cases} \sigma_{ij,j} - \rho_s \omega^2 w = 0 & in\ \Omega_s \\ \nabla^2 p(x) + k^2 p(x) = 0 & in\ \Omega_f \\ \sigma_{ij}.n = -p\delta_{ij}.n_i & on\ \Sigma_s \\ \dfrac{\partial p}{\partial n} = \rho_f \omega^2 w & on\ \Sigma_f \\ \lim\limits_{r\to\infty} r\left(\dfrac{\partial}{\partial_r} - ik\right) p_s = 0 \end{cases} \tag{9}$$

To obtain a unique solution, it is necessary to close the system by considering a radiation boundary condition to take into account the pressure of the scattered wave $p_s = p - p^{inc}$ vanishes far away from the object, in the so-called far field. It is also possible to deal with an interior fluid domain different from the exterior one, filled by air for example, by splitting the Ω_f into two different medium characteristics in the second equation of the global linear system Eq. 9.

4 FINITE ELEMENT METHOD FOR THE ELASTIC STRUCTURE

Using the equation of elastodynamic of the structure Eq. 2, the boundary condition Eq. 5 and the coupling condition Eq. 7, we write the variational formulation of the structure expressed in terms of displacement field:

$$K_{\Omega_S}(\vec{w}, \vec{w'}) - \omega^2 M_{\Omega_S}(\vec{w}, \vec{w'}) + C_{\Sigma_s}(p, w') = F_{\Sigma_s}(\vec{f}, \vec{w'}) \tag{10}$$

where $w' = \overrightarrow{w'}.\vec{n}$ is the normal component of the displacement vector. K_{Ω_S} and M_{Ω_S} are respectively the rigidity and the mass matrices defined by:

$$K_{\Omega_S}(\vec{w}, \overrightarrow{w'}) = \int_{\Omega_s} \sigma_{ij}(\vec{w}).\varepsilon_{kl}(\overrightarrow{w'})d\Omega_s \tag{11}$$

$$M_{\Omega_S}(\vec{w}, \overrightarrow{w'}) = \int_{\Omega_s} \rho_s \vec{w}.\overrightarrow{w'}d\Omega_s \tag{12}$$

F_{Σ_s} is the operator related the mechanical forces defined by

$$F_{\Sigma_s}(\vec{f}, \overrightarrow{w'}) = \int_{\Sigma_s} \vec{f}.\overrightarrow{w'}d\Sigma_s \tag{13}$$

and C_{Σ_s} is related to the coupling matrix with the acoustic defined by

$$C_{\Sigma_s}(p, w') = \int_{\Sigma_s} p.(\overrightarrow{w'}.\vec{n})d\Sigma_s \tag{14}$$

3.1 Modal resolution and Added Mass Matrix

To solve the Eq. 10, usually, a modal analysis of the structure can be used to reduce the CPU time instead of using the physical unknowns, i.e. displacements at every nodes of the mesh of the structure. It consists in computing the modes Ψ_r and their corresponding frequencies ω_r of the structure in a free-free status with no damping by solving:

$$det(K_{\Omega_S} - \omega^2 M_{\Omega_S}) = 0 \tag{15}$$

Both mass and rigidity matrices can be then reduced on that modal basis $\{\Psi_r^i\}_{i=1,..,m}$, m standing for the number of modes used to represent the dynamic behavior of the structure as follows:

$$K_r = \{\Psi_r^i\}^T K_{\Omega_S}\{\Psi_r^i\} \tag{16}$$

$$M_r = \{\Psi_r^i\}^T M_{\Omega_S}\{\Psi_r^i\} \tag{17}$$

The generalized forces are defined by:

$$F_r = \{\Psi_r^i\}^T F_{\Sigma_s} \tag{18}$$

The reduced coupling matrix is defined by:

$$C_r = \{\Psi_r^i\}^T C_{\Sigma_s} \tag{19}$$

and the reduced displacements are defined by:

$$w_r = \{\Psi_r^i\}^T \vec{w} \tag{20}$$

Reduced on the modal basis, the discretized structural equation Eq. 9 in terms of reduced displacements and jump of acoustic pressure becomes:

$$[K_r - \omega^2 M_r]\{w_r\} = \{F_r\} - C_r\{p\} \tag{21}$$

whose dimension is $\boldsymbol{m}\times\boldsymbol{m}$, with $\boldsymbol{m}$ the number of modes only instead of the physical displacements on every nodes of the mesh of the structure.

In the equation Eq. 15, the exterior fluid around the structure is not taken into account so has no effect on the mechanical behavior of the elastic structure. This is the case where the mass of the fluid embedding the structure is negligible compared with the mass of that latter. In aerospace industry for example, the payload made of very light composite panels is not strongly affected by the fluid around which is the air so the modal basis is generally computed using Eq. 15. On the other hand, for marine applications, it is not the same situation. The heavy fluid, the water sea for example for underwater noise, has a strong effect on the mechanical behavior of the structure which needs to be taken into account during the computational method to evaluate the modal basis. Several numerical methods [22, 23] have been developed to compute that added mass matrix and are available nowadays and implemented in commercial FE packages. Added mass may be modelled by acoustic finite elements, as implemented for example in FE software ABAQUS. In the present paper the boundary element method, implemented in the FE software NX Nastran [21], is considered. A brief overview of the well-known theory of the BEM for the computation of added mass matrix is given in [22] allowing direct computation of wetted natural frequencies by solving

$$\boldsymbol{det}\left(\boldsymbol{K}_{\Omega_S}-\boldsymbol{\omega}^2(\boldsymbol{M}_{\Omega_S}-\boldsymbol{M}_A)\right)=\boldsymbol{0} \tag{22}$$

This method will be applied to an academic case of elastic sphere immersed in water. Another way to take into account the strong coupling of the structure in the heavy fluid around consists in solving the direct nodal mechanical system Eq. 10 instead of representing the mechanical behavior though its modal basis. Indeed, for real industrial applications, the modal basis computation is very expensive in terms of CPU time and RAM. It is even more true for the wetted modal basis which is almost impossible for very large industrial problem like a full submarine as illustrated in Fig 1.

3 THE HYBRID FINITE/BOUNDARY ELEMENT METHOD FOR THE ACOUSTIC DOMAIN

Concerning the propagation of the acoustic wave in the unbounded domain, the standard BEM approach or the more recent coupled MLMM as in [ESA ESTEC] can be employed. Nevertheless, even if this method has several positive points, it also has some important weaknesses limiting its use. In this part, we will present the hybrid approach which seems to be more appropriate.

(a)Vertical cut of the mesh of the submarine for the hybrid method (b)Positions of the fictitious surface embedding the obstacle

Figure 3: The fictitious surface for the Hybrid Method.

As illustrated in Fig. 3, the domain of computation $\boldsymbol{\Omega_f}$ is truncated by introducing a fictitious surface $\boldsymbol{\Gamma}$ embedding the initial obstacle like the Infinite Element Method or the FEM coupled with Perfectly Matched Layers. But contrary to the latters, that fictitious surface can be located at any distance $\boldsymbol{r}$ of the obstacle and can take any shape. In the figure Fig. 3, the surface $\boldsymbol{\Gamma}$ is a simple extrusion of the initial surface $\boldsymbol{\Sigma_f}$ of the obstacle along the normal to the surface at $\boldsymbol{r = \lambda/20}$ at 1kHz for example.

By using the integral formulation, we represente the solution at every point in a homogeneous domain by the data of the unknowns on the surfaces on this domain only by using one of the standard three-dimensional integral formulas. Those representations are valid for an exterior acoustic medium $\boldsymbol{\Omega_f}$ with a smooth surface $\boldsymbol{\Sigma_f}$ taking the following forms [5]:

$$\boldsymbol{\phi(x) = \phi_i(x) + V^{*,\Sigma_f}\partial_n p(x) - N^{*,\Sigma_f} p(x),\ x \in \Omega_f} \tag{23}$$

where

$$\boldsymbol{V^{*,\Sigma_f}\partial_n p(x) = \int_{\Sigma_f} G_k(x,y)\partial_n p(y)\, d\Sigma_f(y)} \tag{24}$$

and

$$\boldsymbol{N^{*,\Sigma_f} p(x) = \int_{\Sigma_f} \partial_n G_k(x,y) p(y)\, d\Sigma_f(y)} \tag{25}$$

or

$$\boldsymbol{\partial_n \phi(x) = \partial_n \phi_i(x) + \partial_n V^{*,\Sigma_f}\partial_n p(x) - \partial_n N^{*,\Sigma_f} p(x),\ x \in \Omega_f} \tag{26}$$

where

$$\boldsymbol{\partial_n N^{*,\Sigma_f} p(x) = D^{*,\Sigma_f} p(x)} \tag{27}$$

The free-space Green's function $\boldsymbol{G_k}$ for the Helmholtz equation in the three dimensions is given by

$$\boldsymbol{G_k(x,y) = e^{ik\|x-y\|} \Big/ 4\pi\|x-y\|} \tag{28}$$

where $\boldsymbol{r = \|x-y\|}$ is the distance between the field point $\boldsymbol{x}$ and the moving point $\boldsymbol{y}$ and $\boldsymbol{n}$ is the outward directed normal at $\boldsymbol{y}$. By using the integral representations Eq. 23 and Eq. 26, the radiation boundary condition on $\boldsymbol{\Gamma}$ takes the following form:

$$\boldsymbol{\frac{\partial p}{\partial_n} + ik\eta p = \frac{\partial \phi}{\partial_n} + ik\eta\phi \ on\ \Gamma} \tag{29}$$

with the normal vector $\boldsymbol{n}$ on $\boldsymbol{\Gamma}$ and $\boldsymbol{\Sigma_f}$ pointing inside the domain $\boldsymbol{\Omega_{FEM}}$ defined by $\boldsymbol{\Omega_{FEM} \subset \Omega_f}$ with $\boldsymbol{\partial\Omega_{FEM} = \Gamma \cup \Sigma_f}$. The acoustic equations in the initial system Eq. 9 becomes

$$\begin{cases} \boldsymbol{\Delta p + k^2 p = 0} & \boldsymbol{in\ \Omega_{FEM}} \\ \boldsymbol{\frac{\partial p}{\partial n} = \rho_f \omega^2 w} & \boldsymbol{on\ \Sigma_f} \\ \boldsymbol{\frac{\partial p}{\partial_n} + ik\eta p = \frac{\partial \phi}{\partial_n} + ik\eta \phi} & \boldsymbol{on\ \Gamma} \end{cases} \tag{30}$$

The Sommerfeld radiation boundary condition is replaced by the radiation boundary condition Eq. 29 on $\boldsymbol{\Gamma}$. Applying the standard Finite Element Method by multiplying the Helmholtz system Eq. 25 by a test function $\boldsymbol{p'}$, the variational formulation of the system Eq. 30 and the Eq. 8 provides the following form

$$\begin{gathered} \forall \boldsymbol{p' \in H^1(\Omega_{FEM}),\ find\ p \in H^1(\Omega_{FEM})/} \\ \boldsymbol{H_{\Omega_{FEM}}(p,p') - \omega^2 Q_{\Omega_{FEM}}(p,p') - i\omega B_\Gamma(p,p') +} \\ \boldsymbol{\omega^2 \partial_n V^{\Gamma,\Sigma_f}(w,p') - D^{\Gamma,\Sigma_f}(p,p') + i\omega \frac{\eta}{c}\left(\omega^2 V^{\Gamma,\Sigma_f}(w,p') - N^{\Gamma,\Sigma_f}(p,p')\right) +} \\ \boldsymbol{\omega^2 C_{\Sigma_f}(w,p') = -\frac{1}{\rho_f}(C_\Gamma(\partial_n \phi_i, p') + i\omega \frac{\eta}{c} C_\Gamma(\phi_i, p'))} \end{gathered} \tag{31}$$

with $\boldsymbol{w = \vec{w}.\vec{n} = \frac{1}{\rho_f \omega^2}\frac{\partial p}{\partial n}}$ and where

$$\begin{gathered} \boldsymbol{H_{\Omega_{FEM}}(p,p') = \int_{\Omega_{FEM}} \frac{1}{\rho_f} \nabla p . \nabla p'\, d\Omega} \quad ; \quad \boldsymbol{Q_{\Omega_{FEM}}(p,p') = \int_{\Omega_{FEM}} \frac{1}{\rho_f c^2} p\, p'\, d\Omega} \\ \boldsymbol{B_{\Sigma_f}(p,p') = \int_{\Sigma_f} \frac{\eta}{\rho_f c} p\, p'\, d\Sigma} \quad ; \quad \boldsymbol{C_S(g,p') = \int_S g\, p'\, d\Omega} \end{gathered} \tag{32}$$

and with

$$\begin{gathered} \boldsymbol{V^{\Gamma,\Sigma_f}(w,p') = \int_{\Gamma\times\Sigma_f} w(y) G_k(x,y) p'(x)\, d\Sigma_f(y)\, d\Gamma(x)} \\ \boldsymbol{\partial_n V^{\Gamma,\Sigma_f}(w,p') = \int_{\Gamma\times\Sigma_f} w(y) \partial_{nx} G_k(x,y) p'(x)\, d\Sigma_f(y)\, d\Gamma(x)} \\ \boldsymbol{D^{\Gamma,\Sigma_f}(p,p') = \int_{\Gamma\times\Sigma_f} \frac{1}{\rho_f} p(y) \frac{\partial^2 G_k(x,y)}{\partial n^2} p'(x)\, d\Sigma_f(y)\, d\Gamma(x)} \end{gathered} \tag{33}$$

and

$$\boldsymbol{N^{\Gamma,\Sigma_f}(p,p') = \int_{\Gamma\times\Sigma_f} \frac{1}{\rho_f} p(y) \partial_{ny} G_k(x,y) p'(x)\, d\Sigma_f(y)\, d\Gamma(x)} \tag{34}$$

Discretizinf the Eq. 31 by using the volumic Finite Elements in $\boldsymbol{\Omega_{FEM}}$ and the surfacic Finite Elements on $\boldsymbol{\Sigma_f}$ and $\boldsymbol{\Gamma}$ and combining Eq. 10 and Eq. 31, finally the fully coupled vibro-acoustic fluid structure system expressed in terms of accelleration defined by $\boldsymbol{\vec{\gamma} = -\omega^2 \vec{w}}$ for the structure part is given by

$$\begin{bmatrix} -\frac{1}{\omega^2}[K_{\Omega_S} - \omega^2 M_{\Omega_S}] & C_{\Sigma_s} & 0 & 0 \\ C_{\Sigma_f} & -[H_{\Omega_{FEM}} - \omega^2 Q_{\Omega_{FEM}}]_{\Sigma_f \Sigma_f} & 0 & -[H_{\Omega_{FEM}} - \omega^2 Q_{\Omega_{FEM}}]_{\Omega\Sigma_f} \\ \partial_n V^{\Gamma,\Sigma_f} + i\omega \frac{\eta}{c} V^{\Gamma,\Sigma_f} & D^{\Gamma,\Sigma_f} + i\omega \frac{\eta}{c} N^{\Gamma,\Sigma_f} & -[H_{\Omega_{FEM}} - \omega^2 Q_{\Omega_{FEM}}]_{\Gamma\Gamma} + i\omega B_\Gamma & -[H_{\Omega_{FEM}} - \omega^2 Q_{\Omega_{FEM}}]_{\Omega\Gamma} \\ 0 & -[H_{\Omega_{FEM}} - \omega^2 Q_{\Omega_{FEM}}]_{\Sigma_f \Omega} & -[H_{\Omega_{FEM}} - \omega^2 Q_{\Omega_{FEM}}]_{\Gamma\Omega} & -[H_{\Omega_{FEM}} - \omega^2 Q_{\Omega_{FEM}}]_{\Omega\Omega} \end{bmatrix} \begin{Bmatrix} \vec{\gamma} \\ p_{\Sigma_f} \\ p_\Gamma \\ p_{\Omega_{FEM}} \end{Bmatrix}$$

$$= \begin{bmatrix} F_{\Sigma_s} \\ 0 \\ \frac{1}{\rho_f}([C_\Gamma]\{\partial_n \phi_i\} + i\omega \frac{\eta}{c}[C_\Gamma]\{\phi_i\}) \\ 0 \end{bmatrix} \tag{35}$$

where $\left\{\boldsymbol{p}_{\boldsymbol{\Sigma_f}}, \boldsymbol{p}_{\boldsymbol{\Gamma}}, \boldsymbol{p}_{\boldsymbol{\Omega_{FEM}}}\right\}$ represents respectively the nodal values of the computed pressure on the surface $\boldsymbol{\Sigma_f}$ of the ostacle, on the fictitious $\boldsymbol{\Gamma}$ surface and in the interior of the fluid domain $\grave{\boldsymbol{\Omega}}_{\boldsymbol{FEM}} = \boldsymbol{\Omega_{FEM}} \setminus \left\{\boldsymbol{\Sigma_f} \cup \boldsymbol{\Gamma}\right\}$ and $\{\vec{\boldsymbol{\gamma}}\}$ is the nodal values vector of the computed acceleration of the elastic structure.

The linear system Eq. 35 can be solved by using a direct approach but several difficulties limit this way:

- The left-hand-side (LHS) is composed by both linear sparse and dense operators and mixt operators are not easy to store and to inverse. The only way consists in the Schur Complement of the Sparse part over the dense one.
- The global linear system is not symmetric.
- The dense blocks are treated by standard BEM method whose RAM and CPU time requirements increase as $\boldsymbol{O}(\boldsymbol{N^2})$ and $\boldsymbol{O}(\boldsymbol{N^3})$ to be stored and inversed respectively with $\boldsymbol{N}$ standing for the number of degrees of freedom over the surface $\boldsymbol{\Sigma_f}$ of the obstacle.

The best solution to treat the linear system Eq. 35 relies on a Domain Decomposition Method (DDM) with overlapping ordering the sparse and the dense operators to obtain the following form:

$$\begin{bmatrix} -\frac{1}{\omega^2}\left[K_{\Omega_s} - \omega^2 M_{\Omega_s}\right] & C_{\Sigma_s} & 0 & 0 \\ C_{\Sigma_f} & -\left[H_{\Omega_{FEM}} - \omega^2 Q_{\Omega_{FEM}}\right]_{\Sigma_f\Sigma_f} & 0 & -\left[H_{\Omega_{FEM}} - \omega^2 Q_{\Omega_{FEM}}\right]_{\Omega\Sigma_f} \\ \mathbf{0} & \mathbf{0} & -\left[H_{\Omega_{FEM}} - \omega^2 Q_{\Omega_{FEM}}\right]_{\Gamma\Gamma} + i\omega B_\Gamma & -\left[H_{\Omega_{FEM}} - \omega^2 Q_{\Omega_{FEM}}\right]_{\Omega\Gamma} \\ 0 & -\left[H_{\Omega_{FEM}} - \omega^2 Q_{\Omega_{FEM}}\right]_{\Sigma_f\Omega} & -\left[H_{\Omega_{FEM}} - \omega^2 Q_{\Omega_{FEM}}\right]_{\Gamma\Omega} & -\left[H_{\Omega_{FEM}} - \omega^2 Q_{\Omega_{FEM}}\right]_{\Omega\Omega} \end{bmatrix} \begin{Bmatrix} \vec{\gamma} \\ p_{\Sigma_f} \\ p_\Gamma \\ p_{\Omega_{FEM}} \end{Bmatrix} = \boldsymbol{G}(F_{\Sigma_s}, \phi_i, \partial_n\phi_i, p_{/\Sigma_f}, \partial_n p_{/\Sigma_f}) \tag{36}$$

where

$$\boldsymbol{G}\left(\boldsymbol{F}_{\boldsymbol{\Sigma_s}}, \boldsymbol{\phi_i}, \boldsymbol{\partial_n\phi_i}, \boldsymbol{p}_{\overline{\boldsymbol{\Sigma_f}}}, \boldsymbol{\gamma}\right) = \tag{37}$$

$$\begin{bmatrix} \boldsymbol{F}_{\boldsymbol{\Sigma_s}} \\ 0 \\ \dfrac{\mathbf{1}}{\boldsymbol{\rho_f}}\left([\boldsymbol{C_\Gamma}]\{\boldsymbol{\partial_n\phi_i}\} + \boldsymbol{i\omega}\dfrac{\boldsymbol{\eta}}{\boldsymbol{c}}[\boldsymbol{C_\Gamma}]\{\boldsymbol{\phi_i}\}\right) - \left[\boldsymbol{D}^{\boldsymbol{\Gamma},\boldsymbol{\Sigma_f}} + \boldsymbol{i\omega}\dfrac{\boldsymbol{\eta}}{\boldsymbol{c}}\boldsymbol{N}^{\boldsymbol{\Gamma},\boldsymbol{\Sigma_f}}\right]\left\{\boldsymbol{p}_{\boldsymbol{\Sigma_f}}\right\} - \left[\boldsymbol{\partial_n V}^{\boldsymbol{\Gamma},\boldsymbol{\Sigma_f}} + \boldsymbol{i\omega}\dfrac{\boldsymbol{\eta}}{\boldsymbol{c}}\boldsymbol{V}^{\boldsymbol{\Gamma},\boldsymbol{\Sigma_f}}\right]\{\boldsymbol{\gamma}\} \\ 0 \end{bmatrix}$$

On that form, noting that $\left[\boldsymbol{C}_{\boldsymbol{\Sigma_f}}\right]^{\boldsymbol{t}} = \left[\boldsymbol{C}_{\boldsymbol{\Sigma_s}}\right] = [\boldsymbol{C}]$, the linear system becomes symmetric and completly sparse. In the right-hand-side (RHS), both quantities $\left\{\boldsymbol{p}_{/\boldsymbol{\Sigma_f}} = \boldsymbol{p}_{\boldsymbol{\Sigma_f}}\right\}$ and $\left\{\boldsymbol{\gamma}_{/\boldsymbol{\Sigma_f}} = \boldsymbol{\gamma}\right\}$ are still unknown so the system needs to be solved implicitely by an iterative process. To solve the problem Eq 36 under the saddle point form $\boldsymbol{AX^{(n+1)}} = \boldsymbol{F} - \boldsymbol{BX^{(n)}}$, the standard Gauss-Seidel method can be used. It consists in the following algorithm

$$\begin{cases} \boldsymbol{Define}: \boldsymbol{\varepsilon},\ \boldsymbol{Nb_{iter}}^{\boldsymbol{max}} \\ \boldsymbol{Initiate}: \boldsymbol{n=0},\ \boldsymbol{p_{\Sigma_f}}^{(0)},\quad \boldsymbol{\gamma}^{(0)}, \boldsymbol{p_{\Sigma_f}}^{(1)} \neq \boldsymbol{0}\ \boldsymbol{and}\ \boldsymbol{\gamma}^{(1)} \neq \boldsymbol{0} \\ \boldsymbol{While}\ \left\| \boldsymbol{R}\left(\left\{\boldsymbol{p_{\Sigma_f}}^{(n+1)}, \boldsymbol{\gamma}^{(n+1)}\right\}, \left\{\boldsymbol{p_{\Sigma_f}}^{(n)}, \boldsymbol{\gamma}^{(n)}\right\}\right)\right\| > \boldsymbol{\varepsilon}\ \boldsymbol{and}\ \boldsymbol{n} < \boldsymbol{Nb_{iter}}^{\boldsymbol{max}} \\ \quad (\boldsymbol{1})\ \boldsymbol{Compute}\ \boldsymbol{G_n}\left(\boldsymbol{F_{\Sigma_s}}, \boldsymbol{\phi_i}, \boldsymbol{\partial_n \phi_i}, \boldsymbol{p_{\Sigma_f}}^{(n)}, \boldsymbol{\gamma}^{(n)}\right)\ \boldsymbol{by\ MVP} \\ \quad (\boldsymbol{2})\ \boldsymbol{Solve\ the\ linear\ system\ for}\ \left\{\boldsymbol{p_{\Sigma_f}}^{(n+1)}\right\}\ \boldsymbol{and}\ \left\{\boldsymbol{\gamma}^{(n+1)}\right\} \\ \quad (\boldsymbol{3})\boldsymbol{Compute\ the\ new\ residual}\ \boldsymbol{R}\left(\left\{\boldsymbol{p_{\Sigma_f}}^{(n+1)}, \boldsymbol{\gamma}^{(n+1)}\right\}, \left\{\boldsymbol{p_{\Sigma_f}}^{(n)}, \boldsymbol{\gamma}^{(n)}\right\}\right) \\ \quad (\boldsymbol{4})\ \boldsymbol{n} = \boldsymbol{n+1} \\ \boldsymbol{End\ While} \end{cases} \tag{38}$$

where $\boldsymbol{R(p,q)} = \boldsymbol{\|p-q\|/\|q\|}$ is the residual vector whose norm measures the error of the resolution during the iterative solver. Before starting the resolution of Eq. 36, the FEM LHS, which is completely sparse, is stored/computed and a LU factorisation is done. During the iterative process, at step (1), some matrix-vector products (MVP) are needed to evaluate the new iterate $\boldsymbol{G_{n+1}}$. This step is handled by the MLFMM algorithm; this operation is computed very quickly and with a very low RAM requirement. At step(2), the resolution of the linear system consists only of front/bakcward substitution, the linear system being already factorized at the beginning of the process. Mathematically, it has been demonstrated in [11], [12], [13] the problem Eq. 36 is well-posed and its numerical solution converges towards the solution of the initial problem Eq. 9. It is very interesting to note the first iteration of the process Eq. 38 (with $\boldsymbol{p_{\Sigma_f}}^{(0)} = \boldsymbol{0}\ \boldsymbol{and}\ \boldsymbol{\gamma}^{(0)} = \boldsymbol{0}$) is exactly the FEM formulation with homogenous impedance boundary condition. During the iterative process, the radiation boundary condition will be corrected until it reaches the convergence criteria, that is the reason why this hybrid method is called adaptive absorbing boundary condition (AABC). Consequently, the further from the obstacle the fictitious surface $\boldsymbol{\Gamma}$ is, the faster the iterative solver will converge ($\boldsymbol{N_{iter}^{HYB}}$ will be very small) but the larger the domain of computation $\boldsymbol{\Omega_{FEM}}$ will be. Depending on the computer resources and also the mesh effort the user would like to spend to model the problem, there exists a compromise between both criteria. It has been also demonstrated numerically in [11], [12], [13] the convergence of the iterative process is very fast ($\boldsymbol{N_{iter}^{HYB}} < \boldsymbol{20}$ iterations) even when the surface $\boldsymbol{\Gamma}$ is very close to the obstacle ($\boldsymbol{d} < \boldsymbol{\lambda/100}$). This approach presents all the strengths of the other methods and no weakness:

- The first and main interest of this method is it leads to sparse matrix operators, i.e not fully populated; the RAM requirement to store those sparse operators is $\boldsymbol{O(N)}$ and the complexity to build them is $\boldsymbol{O(N)}$ where $\boldsymbol{N}$ stands for the number of nodes of the mesh descretizing the volumic domain of computation $\boldsymbol{\Omega_{FEM}}$ which can be chosen very small.
- The final equation Eq. 36, which is symmetric, is solved by using the MUMPS library based on a multi-frontal approach which performs a direct $\boldsymbol{LDL^t}$ factorization [4] whose complexity is $\boldsymbol{O(N^2)}$. The direct approach is very well adapted to multiple load cases, i.e. multiple plane waves to compute monostatic TS with a very large number of angles.
- For this method, the domain of computation is quasi-minimal. The fictitious surface $\boldsymbol{\Gamma}$ can be located at any distance from the obstacle and takes any shape.
- The radiation boundary condition is exact on the surface $\boldsymbol{\Gamma}$ at the convergence of the iterative provess.

- The integral operators are never fully allocated and their inversion is not needed. Only some MVP are computed by MLFMM during the iterative process of resolution. Thanks to this method, the RAM requirement to store ab integral operators is on $\boldsymbol{O(N)}$ and the complexity to update the (RHS) is $\boldsymbol{Nlog_{10}^2(N)}$ only.
- Finally, last asset and not the least, the integral operators are no longer singular because the surfaces $\boldsymbol{\Gamma}$ and $\boldsymbol{\Sigma_f}$ are not connected.

To accelerate the convergence of the iterative process, it can be more appropriate to use a Krylov approach rather than a standard Gauss-Seidel method. We design by $\boldsymbol{\Lambda}$ the saddle point operator in Eq. 36 defined by:

$$\boldsymbol{X} = \boldsymbol{\Lambda}(\boldsymbol{X}, \boldsymbol{B}) \tag{39}$$

Consequently, the residual between two iterates is given by

$$\boldsymbol{R} = \boldsymbol{\Lambda}(\boldsymbol{X}, \boldsymbol{B}) - \boldsymbol{X} \tag{40}$$

Because the operator $\boldsymbol{\Lambda}$ is bi-linear in $\boldsymbol{X}$ and $\boldsymbol{B}$, we can write the system in Eq 39 under the following form

$$\boldsymbol{X} - \boldsymbol{\Lambda}(\boldsymbol{X}, \boldsymbol{0}) = \boldsymbol{\Lambda}(\boldsymbol{0}, \boldsymbol{B}) \tag{41}$$

To solve this final system using a Krylov method like the GMRES algorithm, the RHS $(\boldsymbol{\Lambda}(\boldsymbol{0}, \boldsymbol{B}))$ is given by one iteration of the Gauss-Seidel process with initial condition set to zero taken into account the effect of the sources. The MVP $(\boldsymbol{X} - \boldsymbol{\Lambda}(\boldsymbol{X}, \boldsymbol{0}))$ is given by the difference between the current data and result of one iteration of the Gauss-Seidel process by fixing the sources to zero. It is interesting to note that in the linear system Eq 36, the structure can be represented under modal or nodal unknowns depending on the capabilities to compute the modal basis taking into account the added mass effect. When the frequency increases, the modal approach is no more useable and the nodal method is the only solution to model the problem. In this case, both elastic structure and acoustic fluid domain represented by physical unknowns are perfectly managed by a Distributed Memory Processing dedicated sparse linear system like the MUMPS library for example which is able to deal with very large number of unknowns. In the last part, some applications for underwater TS computation for large elastic target are presented to demonstrate the capabilities of that hybrid approach.

4 APPLICATIONS

In this final section, we will present some numerical experiments comparing different approaches and demonstrating the strengths of the coupled hybrid FEM/MLFMM AABC approach.

4.1 Rigid application: the BETSSI-sub model

Since TS data on real submarines is kept confidential, a benchmark model has been designed being realistic enough to provide an accurate measure of real-world performance. It has been developed at Forschungsanstalt der Bundeswehr fur Wasserschall und Geophysik (FWG) in Kiel, Germany in 2002 [14]. The BeTSSi-Sub test case, for Benchmark Target Strength Simulation Submarine, is a 62m x 11m x 7m submarine as illustrated in Fig. 4. For this

simulation, the submarine is considered as rigid. The size of the meshes are presented in Table 1 at 200Hz and 1kHz and in table 4 at 4kHz. All the numerical simulations have been done by using the vibro-acoustic VA One Software [15] developed by ESI Group.

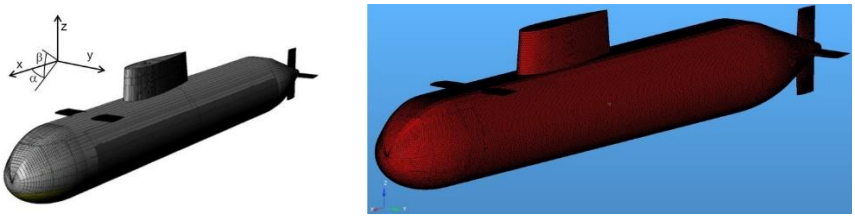

Figure 4: The BeTSSi-Sub test case/The BEM/FMM mesh of the BETSSI model @1kHz.

For each method, the surface $\boldsymbol{\Sigma_f}$ of the obstacle contains 82,263 nodes (164,522 elements). The original shape as well as the details of the submarine are very well taken into account by the mesh whose size is fixed to $\boldsymbol{\lambda/10}$ at 1kHz. The BEM and the MLFMM solvers use exactly the same mesh: only the surface $\boldsymbol{\Sigma_f}$ of the obstacle. The surface $\boldsymbol{\Gamma}$ is only an extrusion of the surface $\boldsymbol{\Sigma_f}$ located at $\boldsymbol{d = \lambda/20}$ at 1kHz for the AABC hybrid FEM-BEM solver. The domain $\boldsymbol{\Omega_{FEM}}$ for the AABC hybrid FEM-BEM solver contains only 164,807 nodes (495,022 elements). From the meshing point of view, this AABC hybrid FEM-BEM method enables a considerable reduction of the domain of computation $\boldsymbol{\Omega_{FEM}}$ in comparison to the mesh which would be needed for the standard FEM coupled with PML or IEM approaches. The same meshes are used for both frequencies: 200Hz and 1kHz.

Table 1: Size of the mesh for each method used at 200Hz and 1kHz.

Methods	Nodes on Σ_f	Nodes on Γ	Nodes in Ω_{FEM}
BEM/MLFMM	82,263	-	-
AABC Hybrid	82,263	82,263	164,807

4.1.1 Bistatic TS

Figures Fig. 4 and Fig. 5 compare the BEM total surface pressure as a reference to the one obtained by the hybrid FEM-BEM for a unit strength plane wave source at a broadside angle ($\boldsymbol{\alpha_i = 90°, \beta_i = 90°}$) and at two frequencies of 200Hz and 1kHz. The results show perfect agreement between both methods. The relative errors of the total pressure field on the surface $\boldsymbol{S}$ computed by the AABC hybrid FEM-BEM method is lower than $\boldsymbol{1}$% for both frequencies with the BEM results considered as a reference. The complexity and the RAM requirements for the different methods are presented in table 2 for 200Hz and 1kHz. The CPU Time and the RAM requirements for the different methods are presented in table 3 for 4kHz for the bistatic TS plane wave source, broadside incidence. For the bistatic TS, it is easy to see the best candidates are the MLFMM and Hybrid FEM/MLFMM AABC in terms of CPU time but also of RAM requirements. For very complex physics (like cavity for example), for very large number of nodes $\boldsymbol{N}$ (so large obstacle and/or high frequencies), the number of iterations needed by the MLFMM solver $\boldsymbol{N_{iter}^{FMM}}$ can be very large (several hundreds) but the number of iteration needed by the Hybrid FEM/MLFMM AABC solver $\boldsymbol{N_{iter}^{HYB}}$ stays low (less than 20).

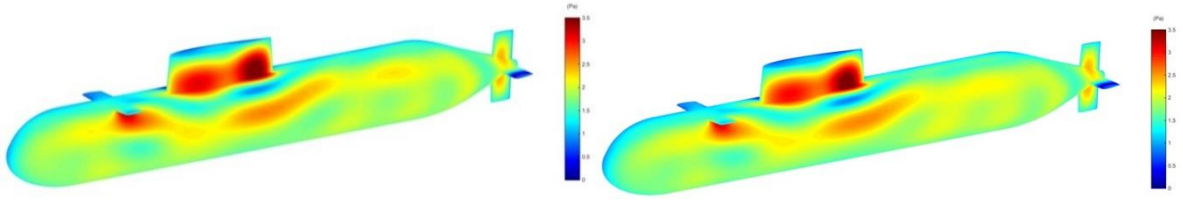

(a) BEM @ 200Hz (b) AABC Hybrid FEM-BEM @ 200Hz

Figure 4: Total acoustic field for the BeTSSi submarine for the BEM (left) and AABC hybrid FEM-BEM (right) from a 200Hz plane wave source, broadside incidence.

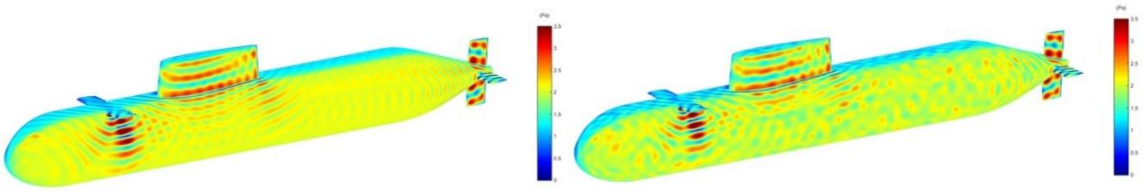

(a) BEM @ 1kHz (b) AABC Hybrid FEM-BEM @ 1kHz

Figure 5: Total acoustic field for the BeTSSi submarine for the BEM (left) and AABC hybrid FEM-BEM (right) from a 1kHz plane wave source, broadside incidence.

Table 2: Complexity and RAM requirements for each method.

Methods	Complexity	RAM (Gb)
BEM	$O(N^3)$	$O(N^2)$
MLFMM	$O(N_{iter}^{FMM} * Nlog_{10}^2(N) * N_{RHS})$	$O(Nlog_{10}^2(N))$
AABC Hybrid	$O(N_{iter}^{HYB} * Nlog_{10}^2(N) * N_{RHS})$	$O(Nlog_{10}^2(N))$

Figures Fig. 6 and Fig. 7 compare both collocation and variational MLFMM total surface pressures as a reference to the one obtained by the hybrid FEM-BEM for a unit strength plane wave source at a broadside angle ($\boldsymbol{\alpha_i = 90°, \beta_i = 90°}$) at the frequency of 4kHz. The collocation MLFMM is used in SMP version with 16 processors whereas the variational MLFMM and hybrid AABC are used in sequential version (with 1 processor only). It is shown in table 3 the hybrid AABC needs the lowest level of RAM (16 Gb only) against both versions of MLFMM (21 and 40 Gb). Concerning the CPU Time, the hybrid AABC method reaches the convergence in only 9 iterations (3h49mn) whereas both MLFMM versions need greater CPU Time (36h15mn in SMP16 for the collocation MLFMM and 78h42mn in sequential for the variational MLFMM). The results show perfect agreement between all the methods. The relative errors of the total pressure field on the surface $\boldsymbol{S}$ computed by the AABC hybrid FEM-BEM method is lower than $\mathbf{1}$% with the variational MLFMM result considered as a reference.

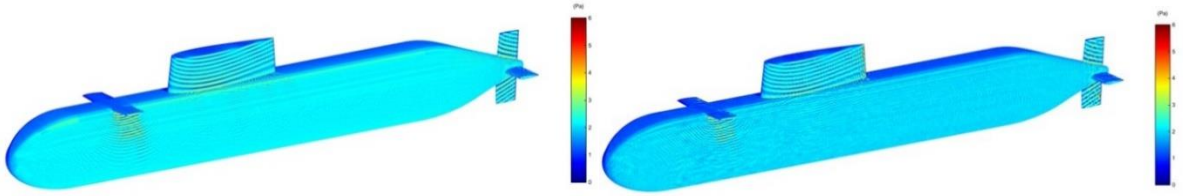

(a) AABC hybrid FEM-BEM @ 4kHz (b) Collocation MLFMM @4kHz

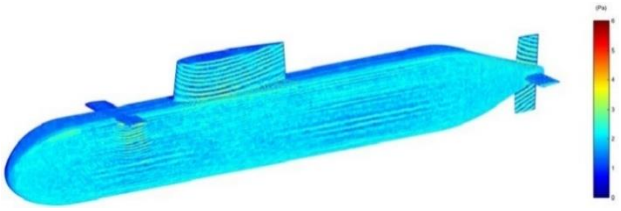

(c) Variational MLFMM @ 4kHz

Figure 6: Total acoustic field for the BeTSSi submarine for the AABC hybrid FEM-BEM (top left), Collocation MLFMM (top right) and Variational MLFMM (down) from a 4kHz plane wave source, broadside incidence.

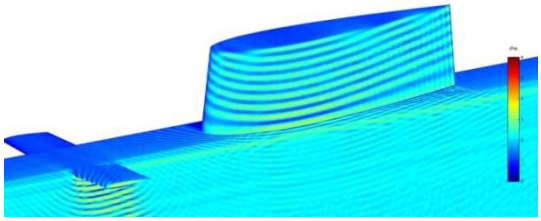

(a) AABC hybrid FEM-BEM @ 4kHz

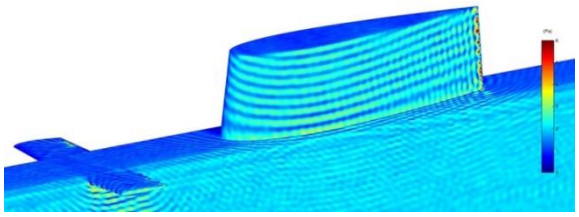

(b) Collocation MLFMM @4kHz

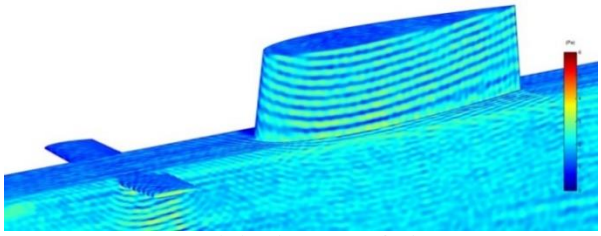

(c) Variational MLFMM @ 4kHz

Figure 7: Total acoustic field for the BeTSSi submarine for the AABC hybrid FEM-BEM (top left), Collocation MLFMM (top right) and Variational MLFMM (down) from a 4kHz plane wave source, broadside incidence.

Table 3: CPU Time and RAM requirements for each method at 4kHz.

Methods	CPU Time	RAM (Gb)
Collocation MLFMM	**36h15mn (459 iterations)**	**40**
Variational MLFMM	**78h42mn (246 iterations)**	**21**
AABC Hybrid	**3h49mn (9 iterations)**	**16**

Table 4: Size of the mesh for each method used at 4kHz.

Methods	Nodes on Σ_f	Nodes on Γ	Nodes in Ω_{FEM}
MLFMM	233,329	-	-
AABC Hybrid	233,329	233,329	467,999

4.1.2 Monostatic TS

Figures Fig. 8 and Fig. 9 show the monostatic TS as a function of backscattered angle for the BeTSSi submarine, as calculated by the acoustic BEM and AABC methods (at 2° increments) for 200Hz and 1kHz which represent respectively a

$\boldsymbol{kL = 52}$ and $\boldsymbol{kL = 260}$. RAYON stands for the deterministic BEM/FEM/AABC solvers inside the VA One software. Also included are the TS results for the BeTSSi submarine model from AVAST software (Acoustic Vibration And STructrual analysis) developed by Martec Ltd., Halifax, Canada [16]. The TS results show very good agreement for 200Hz for all the aspect angle range between AVAST, BEM and AABC. Both BEM and AABC give exactly the same results for 200Hz and 1kHz. Some small differences can be noticed on the second half of the aspect angle range $\boldsymbol{120° < \alpha < 180°}$) for 1kHz. The meshes used for BEM/AABC on one hand and AVAST on the other hand are not the same. In that aspect angle range, the results of the TS are very sensitive to the mesh because of the scattering by the shape of the obstacle (the rudders and the hydroplane blades). The results can be also improved by reducing the aspect angle increments (a $\boldsymbol{2°}$ increment is used for BEM and AABC and probably lower for AVAST).

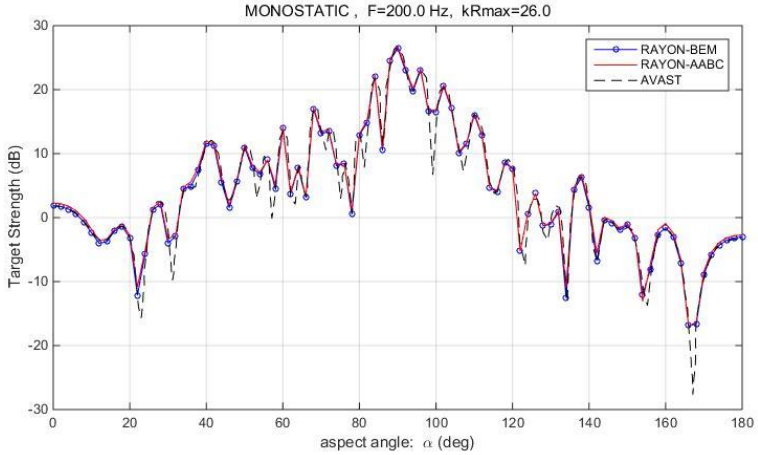

Figure 8: Total acoustic field for the BeTSSi submarine for the BEM (left) and AABC hybrid FEM-BEM (right) from a 200Hz plane wave source, broadside incidence.

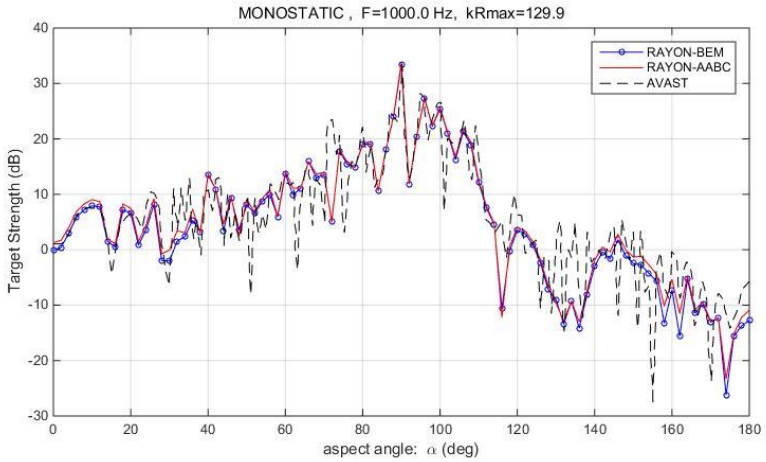

Figure 9: Monostatic target strength as a function of aspect angle for the BeTSSi submarine at a frequency of 1kHz for BEM and AABC method.

Fig. 10 shows finally the monostatic TS as a function of backscattered angle for the BeTSSi submarine, as calculated by the acoustic AABC method (at $\boldsymbol{2°}$ increment) for 4kHz which

represents a $\boldsymbol{kL = 1040}$. Also included are the TS results for the BeTSSi submarine experimental measurements from DSTO (Defense Science and Technology Organisation) Australia [17].

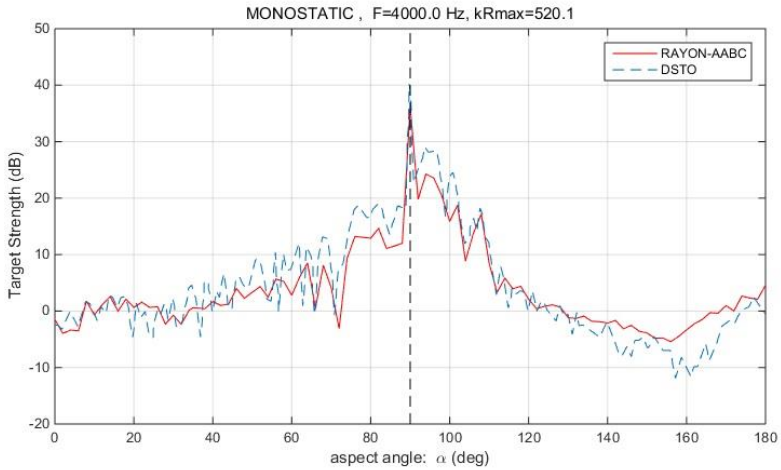

Figure 10: Monostatic target strength as a function of aspect angle for the BeTSSi submarine at a frequency of 4kHz for AABC method.

Comparatively, the AABC Hybrid FEM-BEM method solves the monostatic problem (which is that hardest problem because of the multiple plane waves) about 8 times faster than the BEM using approximately 12 times less memory for both frequencies. The iterative solver Eq. 38 reaches the convergence criteria in only 8 iterations for 200Hz and 14 iterations for 1kHz for $\boldsymbol{\Gamma}$ located at $\boldsymbol{\lambda/20}$ at 1kHz. The MLFMM is comparable to the AABC Hybrid FEM-BEM method for a single plane wave for 200Hz but is the slowest one to deal with the 91 plane waves and for 1kHz for the number of iterations to reach the convergence. The reduced computational and memory requirements of the AABC Hybrid FEM-BEM allow large problems with many unknowns to be solved on desktop PCs. The FEM, the MLFMM and the AABC Hybrid FEM-BEM method run on an i7 2.7GHz processor with 16Gb of RAM on a single processor desktop PC and the BEM method needs to be run on a 2.7GHz processor with 128Gb of RAM on a multiple processors linux machine.

4.2 Fully coupled application: the shell elastic sphere immersed in water

In this example, we will investigate the sound scattered by an elastic spherical shell impinged by an acoustic plane wave. An analytical solution presented in Junger and Feit [27] or [28] is used to validate the accuracy of the results obtained with the presented method.

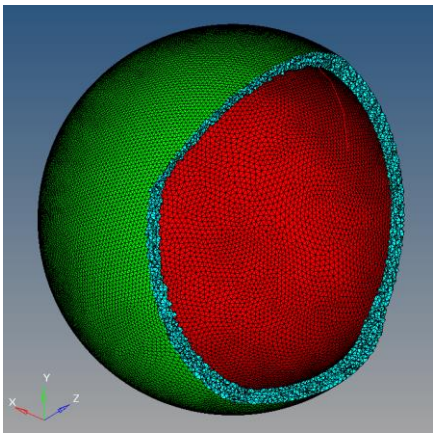

Figure 11: Elastic spherical shell submerged in water Mesh for the AABC hybrid method.

An elastic spherical shell with middle surface radius $\boldsymbol{R = 1\,m}$, thickness $\boldsymbol{h = 0.01\,m}$, and centered at the origin $\boldsymbol{(0,0,0)}$ is considered. A plane wave of amplitude $\boldsymbol{p_0 = 1}$ propagating in the $\boldsymbol{+z}$ direction is scattered by the sphere. The fluid medium surrounding the sphere is assumed to be water with a sound speed of $\boldsymbol{c = 1500\,m.s^{-1}}$ and an ambient density of $\boldsymbol{\rho_f = 1000\,Kg/m^3}$. The spherical shell is assumed to be made of steel with young's modulus $\boldsymbol{E = 195GPa}$, density $\boldsymbol{\rho_s = 7700\,Kg/m^3}$ and poisson's ratio $\boldsymbol{\nu = 0.29}$. We are interested in computing the sound scattered by the elastic sphere at $\boldsymbol{10m}$.

4.2.1 Finite Element Analysis

We performed a modal analysis on unconstrained sphere using the MFLUID card in the NASTRAN finite element software to estimate invacuo modes and natural frequencies. The natural frequencies for the above steel shell in a vacuum and submerged in water, are tabulated in Table **5** and compared between the theory presented in [28] and the numerical results.

The first few natural frequencies along with their degeneracy in parenthesis are 0 Hz (6), 590.11 Hz (5), 698.53 Hz (7), 741.85 Hz (9), etc. The first six modes with zero frequencies belong to the rigid body motions of the sphere. It can be noticed the results are coherent with the theory even in the submerged case.

Table 5: Effect of submergence on the normal modes of a spherical shell.

Mode	In vacuo (theory)	Submerged (theory)	In vacuo (numeric)	Submerged (numeric)
1	0	0	1E-5 (6)	1E-5 (6)
2	589.66	272.15	590.11 (5)	268.59 (5)
3	697.09	343.77	698.53 (7)	347.76 (7)
4	740.07	391.52	741.85 (9)	395.76 (9)
5	761.55	429.71	764.64 (11)	435.07 (11)

6	775.88	458.36	779.77 (13)	463.91 (13)
7	790.20	487.01	792.32 (15)	490.83 (15)
8	802.14	510.88	804.90 (17)	513.93 (17)
9	814.07	534.76	819.32 (19)	537.01 (19)

In total until 1165Hz, 368 modes have been computed for the in vacuo case against 540 modes for the submerged case. It may be seen that radiation loading reduces the natural frequencies of the shell therefore the number of modes representing the machanical behavior of the structure is considerably increased. To compute the modal basis in vacuo, the global CPU time is $\boldsymbol{7mn}$ against $\boldsymbol{1h34mn}$ for the submerged case with 20 CPUs because of the initial computation of the Added Mass Matrix in BEM (outofcore in Nastran) and the impact of that fully populated matrix Added Mass Matrix in the eigen modes algorithm. In terms of CPU time, the wetted modal Hybrid AABC needs $\boldsymbol{28mn}$ and $\boldsymbol{380Mb}$ of RAM whereas the nodal Hybrid AABC needs $\boldsymbol{34mn}$ and $\boldsymbol{851Mb}$ with a sequentiel version.

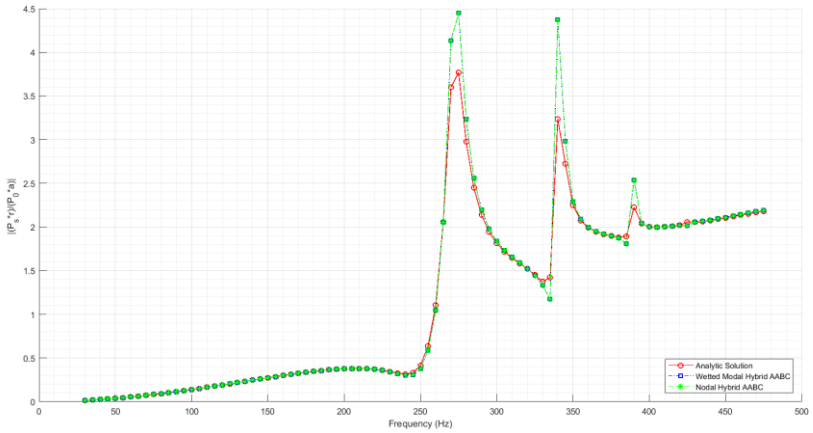

Figure 12: Back scattering by a shell elastic sphere.

Fig. 12 shows the back-scattering at $\boldsymbol{10m}$ (Near TS) as a function of the frequency for the elastic spherical shell. It can be noted both nodal and wetted modal approaches give very coherent results against analytical results. For very large industrial applications when the computation of the wetted modal basis is really expensive, the nodal approach is the only solution to take into account the heavy fluid around the target.

12 CONCLUSIONS

As described, many methods for accurate modeling of the Target Strength of arbitrary shaped objects like a complex submarine are available but they all have some strong limitations coming from computational resources (RAM or CPU time). The AABC hybrid FEM-BEM approach presented in this paper tackles this problem. As shown, this method combines all the strengths of the other methods and presents no weakness. The distance between the fictitious surface supporting the radiation boundary condition and the obstacle is not restricted by the wavelength but rather by the computational resources available. Practically, this distance is fixed equal to

the size of the mesh. By this way, the domain of computation is quasi-minimal. During the iterative process of resolution, only a sparse linear system is solved and the integral operators are involved only through matrix vector products very well adapted to the MLFMM algorithm. Further improvements to the current work, chiefly, the incorporation of high performance computing, will substantially increase its performance reducing the time of computation but also enabling higher frequencies to be reached, up to 8kHz or 10kHz for the rigid BETSI submarine. As presented, the current version of the software is also able to deal with coupled fluid-structure problems and has been applied on a simple academic case with both wetted modal and nodal approaches for the structure part. Nevertheless, it would be interesting to validate it against a more complex industrial case like a real submarine for example. This prototype is also able to deal with a rigid infinite plane to model the ground or an infinite pressure release surface to model the surface of the sea. It would be also interested to model a realistic model of sediments through a rigid infinite plane with an impedance to validate it.

REFERENCES

[1] J.-E. Berenger, "*A perfectly matched layer for the absorption of electromagnetic waves*", [2] Comput. Phys. 114., 185-200, 1994.
[3] Turkel E, Yefet A., "*Absorbing PML boundary layers for wave-like Equations*", Applied Numerical Mathematics, 27(4): 533-557, 1998.
[4] Amestoy and al., "*MUltifrontal Massively Parallel Solver*", Users' guide, 2009.
[5] Shih-AnYang and al., "*Acoustic scattering by a hard or soft body across a wide frequency range by the Helmholtz integral equation method*", J Acoust Soc Am, 102(5):2512–20, 1997.
[6] Balin N., "*Etude de méthodes de couplage pour la résolution des équations de Maxwell : application au calcul de la signature radar d'aéronefs par hybridation de méthodes exactes et asymptotiques*", Thesis, INSA Toulouse, 2005.
[7] J. Dongarra and al., "*LAPACK Users' Guide*", Users' guide, 1999.
[8] G. Sylvand , "*La méthode multipôle rapide en électromagnétisme. Performances, parallélisation, applications*", CERMICS, Thesis, 2000.
[9] E. Darve , "*The Fast Multipole Method I: Error Analysis and Asymptotic Complexity*", SIAM J. Numer. Anal., 38(1), 98-128.
[10] Y. Saad and al , "*GMRES: a generalized minimal residual algorithm for solving nonsymmetric linear systems*", SIAM J. ScI. STAT. COMPUT. Vo|. 7, No. 3, July 1986.
[11] N. Zerbib and al , "*Méthodes de sous-structuration et de décomposition de domaine pour la résolution des équations de Maxwell. Application au rayonnement d'antenne dans un environnement complexe*", Thesis, INSA Toulouse, 2006.
[12] N. Zerbib and al , "*Localized adaptive radiation condition for coupling boundary and finite element methods applied to wave propagation problems*", IMA Journal of Numerical Analysis. 01/2014; 34(3), 2014.
[13] N. Zerbib and al , "*An extension of the adaptive absorbing boundary condition method*", Conference: Antennas and Propagation Society International Symposium, 2007 IEEE.
[14] Ch. Fiedler, H.G. Schneider "*BeTSSi-Sub – Benchmark Target Strength Simulation Submarine*", Technical Report, Forschungsanstalt der Bundeswehr für Wasserschall und Geophysik, Kiel, 2002.

[15] "*VA One: The ONE simulation environment for vibro-acoustic analysis and design*", ESI Group, 2015.
[16] Brennan, D. P. and M. J. Smith, "*Spectral Acceleration Acoustic Modeling and Validation Using AVAST*", Martec Ltd., DREA CR 1999-144, 1999.
[17] Defence Science and Technology Organisation, http://www.dsto.defence.gov.au/, Australian government's lead agency responsible for applying science and technology to safeguard Australia and its national interests.
[18] David S. Burnett, "*A three-dimensional acoustic infinite element based on a prolate spheroidal multipole expansion*", J. Acoust. Soc. Am. 96, 2798 , 1994.
[19] Wilton DT. Acoustic radiation and scattering from elastic structures. Int J Numer Meth Eng. 1978; 13(1):123-138.
[20] Jeans RA, Mathews IC. Solution of fluid-structure interaction problems using a coupled finite element and variational boundary element technique. J Acoust Soc Am.1990; 88(5): 2459-2466.
[21] Merz S, Oberst S, Dylejko PG, Kessissoglou NJ, Tso YK, Marburg S. Development of coupled FE/BE models to investigate the structural and acoustic responses of a submerged vessel. J Comp Acoust. 2007; 15(1): 23-47.
[22] Merz S, Kinns R, Kessissoglou NJ. Structural and acoustic responses of a submarine hull due to propeller forces. J Sound Vib. 2009; 325:266-286.
[23] Peters H, Kessissoglou N, Marburg S. Modal decomposition of exterior acoustic-structure interaction problems with model order reduction. J Acoust Soc Am.2014; 135(5): 2706-2717.
[24] Siemens Software: "NX Nastran Basic Dynamic Analysis User's Guide", 2008.
[25] Louis Armand, Pierre Orsero, A method for evaluating the hydrodynamic added mass in ship hull vibrations, Jean- SNAME Transactions, Vol 87, 1979, pp 99-120
[26] Josip BAŠIĆ, Joško PARUNOV , Analytical and Numerical Computation of Added Mass in Ship Vibration Analysis, Brodogradnja, 64(2):1-11 · June 2013
[27] Miguel C. Junger and David Feit. *Sound, Structures, and their Interaction*, chapter Elastic Scatterers and Wave Guides, Table 9.1, pages 228–234,282,352–358. MIT Press, Cambridge, Massachusetts, second edition, 1986.
[28] C.J. Partridge, MRL Technical Report, MRL-TR-91-10, Sound Wave Scattering from an Elastic Spherical Shell, DSTO, 1993.